Exciton–phonon complexes and optical properties in CdSe nanocrystals

2006 J. Phys.: Condens. Matter 18 7283

(http://iopscience.iop.org/0953-8984/18/31/022)

INSTITUTE OF PHYSICS PUBLISHING JOURNAL OF PHYSICS: CONDENSED MATTER

J. Phys.: Condens. Matter **18** (2006) 7283–7298 doi:10.1088/0953-8984/18/31/022

Exciton–phonon complexes and optical properties in CdSe nanocrystals

E Menéndez-Proupin[1,3], N G Cabo-Bizet[2] and C Trallero-Giner[2]

[1] Departamento de Física, Facultad de Ciencias, Universidad de Chile, Casilla 653, Santiago, Chile
[2] Facultad de Física, Universidad de La Habana, Vedado 10400, La Habana, Cuba

E-mail: emenendez@fisica.ciencias.uchile.cl

Received 4 May 2006, in final form 22 June 2006
Published 21 July 2006
Online at stacks.iop.org/JPhysCM/18/7283

Abstract

A method to calculate the quantum states of exciton–phonon complexes in semiconductor nanocrystals is presented. The exciton–phonon complexes are built from a basis set made of products of phonon states and electron–hole pairs, which are coupled through the electron–phonon Fröhlich interaction, and the electron–hole Coulomb and exchange interactions. In CdSe nanocrystals, the conduction band electrons are described by the effective mass equation, while the holes are represented by the spherical 4×4 Baldereschi–Lipari Hamiltonian. It is shown that a flexible and complete electron–hole basis, not limited to the $1s–1S_{3/2}$ octet, is essential to obtain converged eigenvalues and the correct polaron shift to the exciton energy. A study of the spectral properties is presented; in particular, the spectral region which involves the lowest exciton–phonon complex eigenstates is analysed in details. Specifically, the non-adiabatic nature of the exciton–phonon dynamics in the nanocrystals examined is clearly shown by the vibron eigenstates that were obtained.

1. Introduction

The electron–phonon interaction modulates or determines almost every process in semiconductor systems. While its effects in bulk materials can generally be considered as perturbations, conceptually and technically, this situation can be strongly modified by the inhomogeneity inherent to nanostructures. Two elementary excitations can generally couple unless their interaction is forbidden by symmetry. In particular, the symmetries of time and spatial translation lead in crystal physics to the paradigm of an overlap in energy and wavevector as a natural condition to form coupled states. The breakdown of translational symmetry activates many forbidden interactions; a critical example is the enhancement of the bulk-forbidden Fröhlich electron–phonon interaction [1] in polar semiconductor nanostructures and

[3] Also associate member of the Abdus Salam International Centre for Theoretical Physics.

0953-8984/06/317283+16$30.00

its predominant role in light scattering. Despite this fact, the optical properties of nanostructures have generally been considered as pure electronic transitions assisted by phonon emission or absorption. There are several objections to this picture, at least for zero-dimensional nanostructures. First is the fact that electronic excitations (electrons, holes, excitons) and the optical phonons are all confined in the same region of the space. Second, there are electronic excitations with a high degree of degeneracy, as the lowest exciton in CdSe nanocrystals. Third, there are excitation energies equal to the phonon energies that can be tuned via the size and shape dependence. Although these facts have been noticed in the past [2–7], very limited attempts to study the full spectrum of exciton–phonon coupled states, i.e. the vibrons, have been carried out. Several simplifications have been made, such as parabolic bands [2, 8, 9], neglect of Coulomb effects [10], and two-state exciton models [11]. In all cases, except [11], only the lowest energy level has been studied. In the present work, a method to study the vibrons in CdSe nanocrystals has been developed. The intrinsic complexity of the valence band spectrum of the CdSe nanocrystals is fully described using the Baldereschi–Lipari 4×4 Hamiltonian, and Efros electron–hole exchange and crystal-field splitting operators [12, 13], while the conduction band states are obtained from the effective mass equation. The Coulomb effects in the electronic structure and the vibron states are properly treated using a basis of confined electron–hole pairs (EHP), the completeness of which is controlled by a single cutoff parameter. In section 2 we describe the procedure to build the vibron eigenstates. We monitor the convergence rate by the polaron energy, the phonon occupation number, and a new third parameter which controls the exact convergence of the vibronic states. In section 3 we show the spectral and optical properties of vibron states in a CdSe nanocrystal, and present our final comments. Furthermore, the non-adiabatic character of the electron–phonon dynamics is evidenced by explicitly decomposing important low-lying eigenstates in their substantial and essentially different adiabatic components. The details of the calculation of the excitons and longitudinal optical (LO) phonon modes that originate the vibrons are summarized in the appendix.

2. Theory

2.1. Physical model

The exciton–optical phonons system is described by the Hamiltonian

$$H = H_{\mathrm{E}} + H_{\mathrm{L}} + H_{\mathrm{E–L}} = \sum_{\mu,\mu'} E_{\mu',\mu} \hat{D}^{\dagger}_{\mu'} \hat{D}_{\mu} + \sum_{p} \hbar\omega_{\mathrm{p}} \hat{b}^{\dagger}_{\mathrm{p}} \hat{b}_{\mathrm{p}} + \sum_{\mu,\mu',p} \Big[\langle \mu' | H^{+}_{\mathrm{E–L}}(p) | \mu \rangle \hat{b}^{\dagger}_{\mathrm{p}} + \langle \mu' | H^{-}_{\mathrm{E–L}}(p) | \mu \rangle \hat{b}_{\mathrm{p}} \Big] \hat{D}^{\dagger}_{\mu'} \hat{D}_{\mu}, \tag{1}$$

where H_{E}, H_{L}, and $H_{\mathrm{E–L}}$ are the Hamiltonians of the electronic system, lattice vibrations, and their interaction, respectively. $\hat{D}_{\mu}$ and $\hat{b}_{\mathrm{p}}$ ($\hat{D}^{\dagger}_{\mu}$ and $\hat{b}^{\dagger}_{\mathrm{p}}$) are annihilation (creation) operators of EHPs μ and phonons p. The electronic matrix elements $E_{\mu',\mu}$, the phonon energies $\hbar\omega_{\mathrm{p}}$, and the EHP-phonon matrix elements are discussed in the appendix. Note that the μ states can be any excited states of the electronic system, the ground state of which (vacuum) is taken as fully occupied valence bands and an empty conduction band. In a wide-gap semiconductor, such as CdSe, the energy required for creating an exciton from the vacuum or a biexciton from an exciton is much larger than the phonon energies. Hence, we ignore contributions of biexcitons and the vacuum to the vibron states.

Due to the spherical symmetry, the EHP states $|\mu\rangle$ can be described by the quantum numbers of the energy N_{μ}, the total angular momentum M_{μ}, its projection on the Z-axis $M_{z\mu}$,

and the parity $P_\mu = \pm 1$ (see appendix and [14]). Due to the spherical symmetry, the phonons are labelled by the indices $p \equiv (\tilde{n}_\mathrm{p}, l_\mathrm{p}, m_\mathrm{p})$ [15], which can be considered as quantum numbers of energy, angular momentum, and its projection. Note that we use $\tilde{n}_\mathrm{p}$ for the normal mode index, and reserve n_p for the phonon occupation number.

Once the EHPs and the phonons are calculated, the vibrons can be obtained by a series expansion

$$|v\rangle = \sum_{\mu;n_{p_1},n_{p_2},\ldots} t(v)_{\mu;n_{p_1},n_{p_2},\ldots} \left|n_{p_1}, n_{p_2}, \ldots; \mu\right\rangle, \tag{2}$$

where $t(v)_{\mu;n_{p_1},n_{p_2},\ldots}$ are variational coefficients and

$$\left|n_{p_1}, n_{p_2}, \ldots; \mu\right\rangle = \frac{(\hat{b}^\dagger_{p_1})^{n_{p_1}}}{\sqrt{n_{p_1}!}} \frac{(\hat{b}^\dagger_{p_2})^{n_{p_2}}}{\sqrt{n_{p_2}!}} \ldots \hat{D}^\dagger_\mu |0\rangle. \tag{3}$$

Applying the Hamiltonian (1) to the state (2), the eigenvalue problem can be transformed into the numerical diagonalization of the Hermitian matrix

$$\begin{aligned}\left\langle \mu'; n'_{p_1}, n'_{p_2}, \ldots\right| H \left|n_{p_1}, n_{p_2}, \ldots; \mu\right\rangle &= [E_{\mu',\mu} + (n_{p_1}\hbar\omega_{p_1} + n_{p_2}\hbar\omega_{p_2} + \cdots)\delta_{\mu,\mu'}] \\ &\times \delta_{n_{p_1},n'_{p_1}} \delta_{n_{p_2},n'_{p_2}} \cdots + \sum_p \Big[\left\langle \mu' \left| H^+_{\mathrm{E–L}}(p)\right| \mu\right\rangle \langle n'_{p_1}, n'_{p_2}, \ldots |\hat{b}^\dagger_\mathrm{p}| n_{p_1}, n_{p_2}, \ldots\rangle \\ &+ \left\langle \mu' \left| H^-_{\mathrm{E–L}}(p)\right| \mu\right\rangle \langle n'_{p_1}, n'_{p_2}, \ldots |\hat{b}_\mathrm{p}| n_{p_1}, n_{p_2}, \ldots\rangle\Big].\end{aligned} \tag{4}$$

The vibron basis $\{|n_{p_1}, n_{p_2}, \ldots; \mu\rangle\}$ should contain the possible EHP states μ and all normal modes p of the nanocrystal with all possible occupation numbers n_{p_i} $(i = 1, 2, \ldots)$. In practice, the basis becomes very large and the key issue is to study the convergence and to find which basis states are essential for the vibrons to be calculated. We present this analysis in section 2.2.

The main technical difficulty is the large dimension of the matrix Hamiltonian. Considering vibrational states of $N_\mathrm{ph} \leqslant (N_\mathrm{ph})_\mathrm{max}$ phonons in N_modes normal modes and N_EHP electron–hole pairs, the dimension of the Hamiltonian matrix is

$$N_\mathrm{matrix} = N_\mathrm{EHP} \times \sum_{N_\mathrm{ph}=0}^{(N_\mathrm{ph})_\mathrm{max}} \frac{(N_\mathrm{modes} + (N_\mathrm{ph})_\mathrm{max} - 1)!}{(N_\mathrm{modes} - 1)! N_\mathrm{ph}!}. \tag{5}$$

As will be shown later, the most stringent parameter to achieve convergence with the basis size is N_EHP, which is related to the electron–hole interaction.

The spherical symmetry allows us to separate the Hamiltonian matrix in blocks. When a phonon is created or annihilated in a process described by $H_\mathrm{E–L}$, there are selection rules that imply the conservation of the parity, the angular momentum projection on the Z-axis, and its square. This was shown explicitly in [16] for the case of a non-degenerate valence band, and it is deduced in a similar way considering the 4×4 Baldereschi–Lipari Hamiltonian and the matrix elements reported in [17]. We take advantage of the symmetry, separating the basis states in groups with well-defined values of the first two conserved magnitudes, i.e.

$$M_v = M_z + \sum_p n_\mathrm{p} \times m_\mathrm{p} \tag{6}$$

for the angular momentum and

$$P_v = (-1)^{1+l+L+\sum_p n_\mathrm{p} \times l_\mathrm{p}} \tag{7}$$

for the parity. In equation (7), l and L are the orbital quantum numbers of the electron and the hole, respectively. The exponent 1 comes from the symmetry of the valence Bloch functions. In order to have a well-defined square of the total angular momentum, we would need to build

symmetrized combinations using the Clebsch–Gordan coefficient. We have not attempted that, in view of the difficulties raised by handling a variable number of particles.

Despite the reduction of the Hamiltonian matrix using (6) and (7), its size does not allow us to calculate all the matrix elements in a reasonable time. Hence, we apply the perturbative method of Löwdin [18] to obtain an effective Hamiltonian matrix of reduced dimension. The basis states (3) can be divided in two groups, let us say, A and B. In group A are included the N_A EHPs (near states) of lowest energy and all possible phonons. In group B are included the remaining EHP with all phonons. Schematically, the vibron state is expanded as

$$|v\rangle = \sum_{i\in A} t_i|\psi_i\rangle + \sum_{\beta\in B} t_\beta|\psi_\beta\rangle, \tag{8}$$

abbreviating $|\psi_i\rangle$, $|\psi_\beta\rangle$ as the basis states. Let h_{ij} be the initial interaction matrix, E_v^0 an approximation to the energy of $|v\rangle$, and let h'_{ij} be a renormalized matrix

$$h'_{ij} = h_{ij} + \sum_{\beta\in B} \frac{h_{i\beta}h_{\beta j}}{E_v^0 - h_{\beta\beta}}, \qquad i, j \in A. \tag{9}$$

Then the energies E_i and the coefficients t_i can be obtained from the equation

$$\sum_{j\in A}(h'_{ij} - E_i\delta_{ij})t_j = 0, \qquad i, j \in A \tag{10}$$

and

$$t_\beta = \sum_{k\in A} \frac{h_{\beta k}}{E_v^0 - h_{\beta\beta}}, \qquad \beta \in B, \quad k \in A. \tag{11}$$

In principle, the energies E_i are obtained by a self-consistent solution of equations (9) and (10). In this work, self-consistence has not been used, but a reasonable approximation to the full diagonalization results is obtained. As an initial approximation E_v^0 for the polaron energy, we have chosen either the term h_{11} or the lowest eigenvalue of h_{ij} ($i, j \in A$), obtaining practically equal results. The number of near EHP states (N_A) must be chosen by a compromise between accuracy and the expense of computer resources. It must satisfy two constraints. First, all the EHPs with an energy in the spectral range of interest must be included in group A. Second, group A must include only closed shells of EHPs in order to preserve the fine structure of the vibron levels.

2.2. Vibron basis and convergence control

As we are proposing a new method to find the eigenstates of the Hamiltonian (1), it is very important to evaluate its ability to provide the correct eigenstates and its accuracy. We shall see that some physical parameters, i.e. the polaron correction energy, have stringent convergence requirements. We need to establish which phonon and EHP states must be included in the vibron basis to get reasonable physical properties for the lowest-energy vibrons. For CdSe nanocrystals we use the parameters listed in table 1.

First, we have determined the multiphonon states that must be included in the basis. We build the vibron basis, adding states of zero phonons (which are the pure EHPs), one phonon, two phonons, etc, up to a maximum phonon population $(N_{\mathrm{ph}})_{\max} = \max(n_{p_1} + n_{p_2} + \cdots)$. We have included in the basis the optical phonons with $\tilde{n}_{\mathrm{p}} = 1$, $0 \leqslant l_{\mathrm{p}} \leqslant 3$, and $-l_{\mathrm{p}} \leqslant m_{\mathrm{p}} \leqslant l_{\mathrm{p}}$. To monitor the convergence, we have used the energy, the mean phonon occupation number $\langle n\rangle = \sum_p \langle v|\hat{b}_{\mathrm{p}}^\dagger\hat{b}_{\mathrm{p}}|v\rangle$, and the number $\Lambda = (1/\hbar\omega_{\mathrm{LO}})\sum_p \left|\langle v|[\hat{b}_{\mathrm{p}}, \hat{H}]|v\rangle\right|$. The estimator Λ has the advantage that we know its exact value when $|v\rangle$ is an exact eigenstate of $\hat{H}$, i.e. zero. We have made test calculations with $0 \leqslant (N_{\mathrm{ph}})_{\max} \leqslant 5$, keeping fixed the number of EHPs in

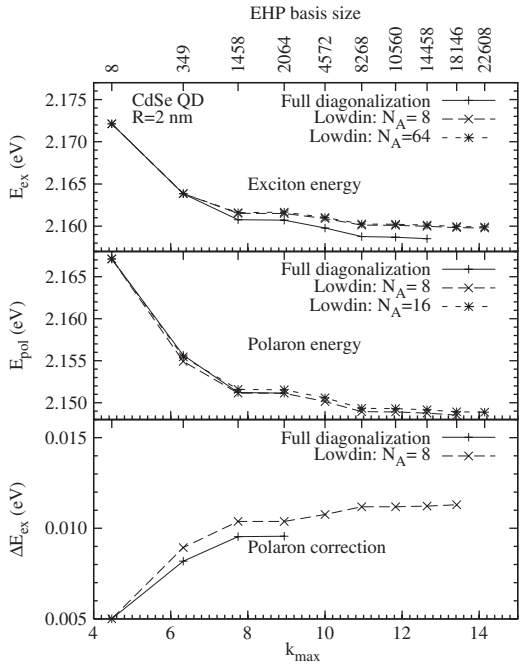

Figure 1. Convergence of the exciton and polaron energies, and its difference (polaron correction) with the size of the electronic basis for a CdSe quantum dot 2 nm in radius. The basis set contains zero-, one- and two-phonon states. The full diagonalization results are compared with the Löwdin scheme, where N_A is the number of near EHP states.

the basis, and we have found that, for $(N_{\rm ph})_{\rm max} = 2$, the energy converges within 0.1 meV, $\langle n \rangle$ within 0.02, and $\Lambda \sim 0.03$. The results are identical for $M_z = 0, 2$, and if the maximum phonon $l_{\rm p}$ is 2 or 3. This means that $l_{\rm p} = 3$ phonons are not important for the lowest-energy vibrons.

We generate the EHP basis, taking all the electron and hole wavefunctions with wavenumbers k smaller than a cutoff $k_{\rm max}$. Hence, the cutoff energies for electrons and holes are $E_{\rm cut}({\rm e,h}) = \hbar^2 k_{\rm max}^2 / 2 m_{\rm e,hh} R^2$, respectively. This scheme is more efficient than using a single cutoff for the electrons and holes. As the electron wavefunctions are modelled using an effective radius $R_{\rm eff}$, the cutoff wavenumber for them is slightly reduced, according to $\tilde{k}_{\rm max} = k_{\rm max} R / R_{\rm eff}$. Figure 1 shows the convergence of the lowest energy of the bare exciton (i.e. including only zero-phonon states in the basis) and the polaron (lowest vibron) including up to two phonon states. The difference between these energies (polaron correction) is also shown. Figure 1 also shows the comparison between the direct diagonalization of the Hamiltonian and the Löwdin method, which is the only practical way for a large EHP basis. Two facts are remarkable. (1) The large number of EHP basis functions needed to achieve a convergence (relative to the increase of $N_{\rm EHP}$) within 1 meV accuracy. (2) The converged polaron correction $\Delta E_{\rm ex}$ to the exciton energy is 11 meV, doubling the estimation of 5 meV obtained using the EHP basis limited to the 1s–$1S_{3/2}$ octet. This is somewhat surprising, as the diameter of this nanocrystal is smaller than the bulk exciton radius. In fact, it is influenced by the finite confinement acting on the electron, which causes the electron wavefunction to extend up to 2.8 nm from the centre of the nanocrystal. We have repeated the study of convergence, considering infinite confinement for the electron, as well as for the hole, and we find $\Delta E_{\rm ex} = 0.4$ meV[Note 4] using the EHP basis limited to the 1s–$1S_{3/2}$ octet, as in [10]. On the other hand, using the large EHP basis, we get $\Delta E_{\rm ex} \sim 7$ meV. These numbers can be compared with those of Oshiro *et al* [9, 23], of 6 meV for infinite confinement,

[4] This small value is the net effect of the valence band mixing. The corresponding value in a parabolic valence band model is 0.

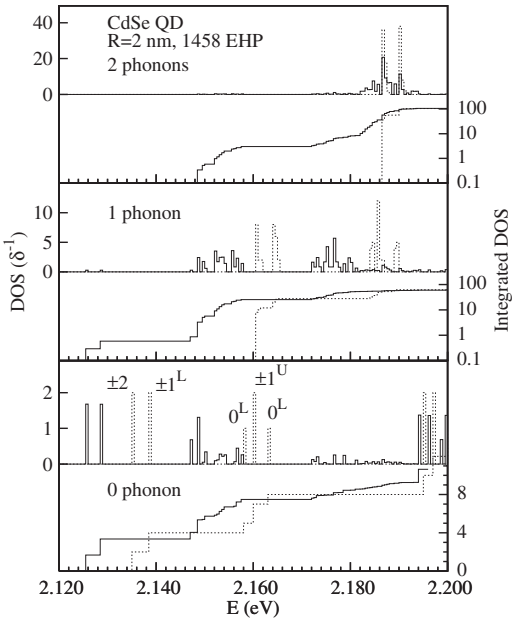

Figure 2. Contributions of $N_{\rm ph}$-phonon states ($N_{\rm ph} = 0, 1, 2$) to the density of states in a wurtzite CdSe nanocrystal 2 nm in radius. The partial DOS are given in units of the inverse of the histogram energy step $\delta = 0.5$ meV. The EHP basis size is defined by $N_{\rm EHP} = 1458$ ($k_{\rm max} = 7.75$) and $N_A = 16$. The full lines show the DOS (up section of each $N_{\rm ph}$ phonon graph) and the integrated DOS (down section of each $N_{\rm ph}$ phonon graph) of vibron states. For comparison, the dotted line shows the combined DOS of pure excitons and phonons. The pure exciton states of the lowest octet are indicated: ± 2, $\pm 1^{\rm L}$, $0^{\rm L}$, $\pm 1^{\rm U}$, $0^{\rm U}$.

and 50–10 meV considering confinement potential, obtained assuming parabolic bands and a variational wavefunction for the exciton. All these facts show the necessity of a flexible basis set and the importance of controlling the convergence.

3. Vibron properties

3.1. Spectral properties

Let us explore the features of the exciton–phonon complexes. It is important to know which phonons couple strongly with the exciton states, the relative contributions of N-phonon states, and to what extent are the coupled states realized in a typical nanocrystal.

First, let us examine the $N_{\rm ph}$-partial density of states (DOS) defined as

$$\rho_{N_{\rm ph}}(E) = \sum_{v} \sum_{\substack{\mu;n_{p_1},n_{p_2},\ldots \\ (n_{p_1}+n_{p_2}+\cdots=N_{\rm ph})}} |t(v)_{\mu;n_{p_1},n_{p_2},\ldots}|^2 \delta(E - E_v). \tag{12}$$

Figure 2 shows, in continuous lines, the vibron $N_{\rm ph}$-partial DOS for a wurtzite CdSe QD 2 nm in radius, calculated using a basis of 1458 EHPs ($k_{\rm max} = 7.75$), 16 of which are the near states in the Löwdin scheme. The dotted lines show the corresponding DOS in the case that the exciton–phonon coupling is dropped. To avoid plotting the delta functions in (12), the $\rho_{N_{\rm ph}}(E)$ are represented by histograms with an energy step $\delta = 0.5$ meV. The DOS are given in units of δ^{-1}, indicating directly the number of states in each step. The energy-integrated

Table 1. Parameters used in the calculations. ϵ_d is the dielectric constant of the glass matrix.

Parameter	CdSe
E_g (eV)	1.841[c]
m_e/m_0	0.13[d]
γ_1	1.66[d]
γ_2	0.41[d]
$2m_0P^2$ (eV)[a]	20[e]
V_e (eV)	0.6[d]
V_h (eV)	∞[d]
Δ (eV)	0.025[f]
$\varepsilon_{exch}a_0^3$ (eV Å^3)	35.81[f]
ϵ_0	9.53[g]
ϵ_∞	5.73[b]
ϵ_d	4.64[g]
ω_L (cm^{-1})	213.1[g]
ω_T (cm^{-1})	165.2[g]
β_L	1.576×10^{-6} [g]
β_T	0[g]

[a] $P = -i\langle S|\hat{p}_x|X\rangle/m_0$.
[b] $\epsilon_\infty = \epsilon_0(\omega_{TO}/\omega_{LO})^2$.
[c] Reference [19].
[d] Reference [20].
[e] Reference [21].
[f] Reference [12].
[g] Reference [22].

partial DOS are also shown, as they are nearly independent of the energy step. In the sum are included the 20 lowest vibron states for each set of quantum numbers $M_v = 0, \pm1, \pm2$ and $P_v = \pm1$. In the absence of the electron–hole interaction and of the coupling with the phonon field, the lowest level is composed of the 1s–1S$_{3/2}$ EHPs. The 1s electron has a spin degeneracy of 2, and the 1S$_{3/2}$ hole has a degeneracy of 4 (neglecting the crystal field splitting), giving an eightfold degeneracy. Their spherical-symmetrized combinations $(1s–1S_{3/2})_{M,M_z}$ have total angular momenta $M = 1$ and 2. The Coulomb interaction does not split this level, but the exchange interaction and the crystal field split it into five levels that are named briefly by their angular momentum projection as ±2, $\pm1^L$, 0^L, $\pm1^U$, and 0^U, with L and U meaning lowest and upper, respectively [13]. Additional peaks show up at energies larger than 2.192 eV coming from the 1s–1P$_{3/2}$ EHP octet. The integrated zero-phonon partial DOS of the uncoupled exciton–phonon system displays steps of integer values at the exciton energies, as it is the DOS of an isolated exciton system. The DOS in the upper panels are the one- and the two-phonon replicas of the exciton DOS. Comparing the bare exciton and vibron DOS, one can appreciate the effects of the exciton–phonon coupling. The effects of the electron–phonon coupling are to shift and to spread the bare exciton levels. The uncoupled one-phonon integrated DOS is 0 for energies smaller than 2.160 eV, however it takes finite values at the polaron energy in the coupled case. For well-separated vibron levels, such as the first two levels, the relative values of the zero- and one-phonon DOS indicate the relative weight of the zero- and one-phonon basis in the composition of the vibron states. The two-phonon integrated DOS is almost zero for an energy smaller than 2.187 eV in the uncoupled case, but rises at 2.148 eV in the coupled case. Comparing the zero- and one-phonon DOS, one sees that the uncoupled exciton $\pm1^U$ at 2.160 eV coincides with the rise of the one-phonon uncoupled DOS. This resonance causes strongly non-adiabatic vibrons when the coupling is switched on.

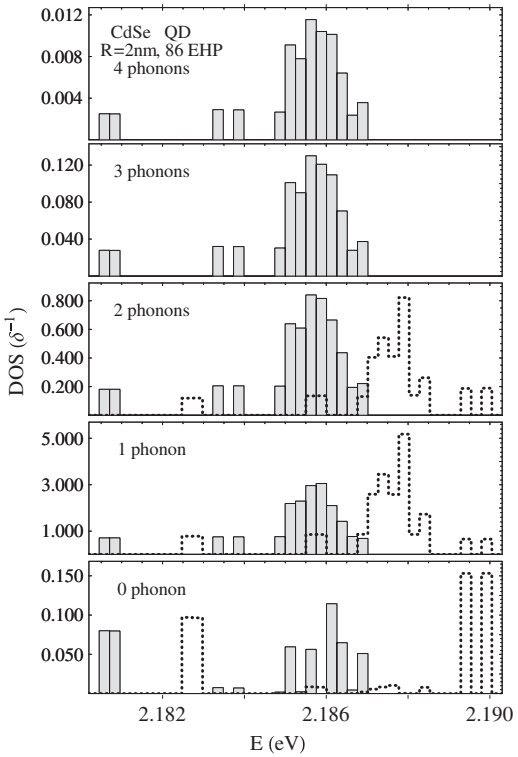

Figure 3. Partial DOS for $N_{\rm ph} = 0, 1, 2, 3, 4$ using a basis with 86 EHP. The first strongly coupled vibrons, from the third excited level to the 28th for $M_v = 0$, are shown. The DOS are given in units of the inverse of the energy step $\delta = 2.525 \times 10^{-4}$ eV. Dotted lines shows the vibron states obtained for a basis with $(N_{\rm ph})_{\rm max} = 2$; the filled curve shows the same states for a basis constructed with $(N_{\rm ph})_{\rm max} = 4$.

3.2. Non-adiabatic properties

Let us consider in more detail the spectral region of one-phonon replicas of the lowest exciton octet. For this study, we include up to four-phonons states in the vibron basis, a reduced set of 86 EHP, and we drop the crystal field and exchange interactions. This extended basis regarding the phonon number allows us to assess the completeness of a two-phonon basis for this spectral region. Also, the phonons ($\tilde{n}_{\rm p} = 2, l_{\rm p} = 0, m_{\rm p} = 0$) and ($\tilde{n}_{\rm p} = 1, l_{\rm p} = 3, m_{\rm p}$) have been included in this basis.

Let us first analyse the influence upon the vibron spectrum of the maximum phonon population $(N_{\rm ph})_{\rm max}$ allowed in the basis set. In figure 3 we show the partial DOS for vibrons with $M_v = 0$. Dotted and full bars correspond to $(N_{\rm ph})_{\rm max} = 2$ and 4, respectively. In the spectral range shown (2.180–2.190 eV), the effect of increasing $(N_{\rm ph})_{\rm max}$ from 2 to 4 is more pronounced than that of the first two-fold degenerate level with $M_v = 0$ (not shown). The one-phonon partial DOS ($N_{\rm ph} = 1$) is the dominant one, and is red-shifted by nearly 2 meV. However, the overall partial DOS profile is not changed significantly. The second leading contribution in this spectral range comes from two-phonon states, followed by zero- and three-phonon states, while the four-phonon partial DOS is one order of magnitude smaller. A significant feature seen in figure 3 is that the shapes of the $N_{\rm ph}$-partial DOS in the plotted range coincide for $N_{\rm ph} = 2, 3, 4$. The inspection of the eigenvectors corresponding to each vibronic

Table 2. Leading contributions to the norm of the lowest non-adiabatic vibron, calculated with $(N_{\mathrm{ph}})_{\max} = 4$.

Basis state	$\lvert t(v)_{\mu;n_{p_1},n_{p_2},\ldots}\rvert^2$	
$\lvert n_{\mathrm{p}};(\text{electron–hole})_{M,M_z}\rangle$	$R = 2.0$ nm	$R = 3.2$ nm
$\lvert 0;(1\mathrm{s}\text{–}1\mathrm{P}_{3/2})_{1,0}\rangle$	0.08	0.42
$\lvert 1_{1,1,-1};(1\mathrm{s}\text{–}1\mathrm{S}_{3/2})_{1,1}\rangle$	0.30	0.20
$\lvert 1_{1,1,1};(1\mathrm{s}\text{–}1\mathrm{S}_{3/2})_{1,-1}\rangle$	0.30	0.20
Other	0.32	0.18

level shows us the mixture between the different basis states. The two lowest degenerate states for $M_v = 0$ at energy 2.160 eV can be approximately considered as adiabatic excitations. From the discussion in section 2.2 and our calculation for $(N_{\mathrm{ph}})_{\max} = 4$, it is clear that the main components of these two vibrons are basis states with 0 phonons, but also important components with different number of phonons ($N_{\mathrm{ph}} = 1, 2$) are present. Nevertheless, the three main contributions corresponds to a certain occupation number of phonons, and a coincident single EHP (for the polaron, this corresponds to the $(1\mathrm{s}\text{–}1\mathrm{S}_{3/2})_{1,0}$ EHP). Thus, these two levels can be considered as adiabatic to a good approximation.

A different picture arises when we study higher states. Almost all the states in the higher spectral range have an important mix of basis states with different EHPs and phonon constituents. For example, the three main components of the third vibron state for $M_v = 0$ (2.181 eV) are the $(1\mathrm{s}\text{–}1\mathrm{P}_{3/2})_{1,0}$ EHP with 0 phonons and the $(1\mathrm{s}\text{–}1\mathrm{S}_{3/2})_{1,M_z}$ ($M_z = \pm 1$) EHPs with one phonon ($\tilde{n}_{\mathrm{p}} = 1, l_{\mathrm{p}} = 1, m_{\mathrm{p}} = -M_z$). Table 2 shows the contributions to the norm of these three basis states. Thus, this level is a non-adiabatic excitation, and this feature is also present in most of the states shown in figure 3. There are no significant differences in the composition of the vibron states obtained with either the reduced basis ($(N_{\mathrm{ph}})_{\max} = 2$) or the extended basis ($(N_{\mathrm{ph}})_{\max} = 4$, and phonons ($\tilde{n}_{\mathrm{p}} = 2, l_{\mathrm{p}} = 0, m_{\mathrm{p}} = 0$) and ($\tilde{n}_{\mathrm{p}} = 1, l_{\mathrm{p}} = 3, m_{\mathrm{p}}$)). The relative weights of the different contributions change with the nanocrystal radius and can undergo a resonance effect. For a radius of 3.2 nm, the energy difference between the two lowest pure exciton levels (calculated considering $(N_{\mathrm{ph}})_{\max} = 0$) equals the LO phonon energy. This produces an increase in the mixing of these states, as can be seen in table 2, while the two-phonon contributions are reduced. It should be remarked that the crystal field and exchange interactions affect the exciton fine structure and modify the values of the wavefunction coefficients. However, it does not alter the above conclusion about the presence of non-adiabatic states associated with the phonon dynamics in CdSe quantum dots.

3.3. Optical properties

Absorption and luminescence spectra in nanostructures are associated with optical transitions between vibronic states. Let us call *down* the energy levels E_{d}, the initial states in photon absorption and the final states in emission. Similarly, let us call *up* the energy levels E_{u}, the final vibron levels in absorption and the initial levels in emission. *Down* levels correspond to the ground electronic state $|G\rangle$ with phonon excitations, the lowest level corresponding to the phonon vacuum. *Up* levels are made of the vibrons calculated in this work.

Neglecting the direct photon–phonon interaction, which is not resonant at optical frequencies, the *up–down* state optical dipole matrix element can be cast as

$$\mathbf{D}_{u,d} = \sum_{\mu;n_{p_1},n_{p_2},\ldots} t(u)^*_{\mu;n_{p_1},n_{p_2},\ldots}\delta_{n'_{p_1},n_{p_1}}\,\delta_{n'_{p_2},n_{p_2}}\ldots\mathbf{D}_{\mu,G}, \tag{13}$$

where $n'_{p_1}, n'_{p_2}, \ldots$ are the phonon occupation numbers of the *down* state. The dipole operator matrix element between an EHP $\mu = |nNlLfF; MM_z\rangle$ and the electronic ground state G is

given by [17]

$$\mathbf{D}_{\mu,G} = \frac{\mathrm{i}e}{m_0\omega_{\mu,G}}\langle\mu\left|\hat{\mathbf{p}}\right|G\rangle \tag{14}$$

$$= \delta_{M,1}\hat{\mathbf{e}}^*_{M_z}\frac{2\mathrm{i}eP}{\omega_{\mu,G}}(-1)^{f+5/2}\sqrt{\frac{(2f+1)(2F+1)}{3}} \times \begin{Bmatrix} 1 & 3/2 & 1/2 \\ l & f & F \end{Bmatrix}\left(\delta_{l,L}+\delta_{l,L+2}\right)\int R^{(F)}_{N,l}(r)R_{nl}(r)r^2\,\mathrm{d}r, \tag{15}$$

where m_0 is the free electron mass, e is the proton charge, and $P = -\mathrm{i}\langle S|p_z|X\rangle/m_0$ is the interband matrix element. These dipole matrix elements are different from zero only for $M = 1$ and proportional to $\hat{\mathbf{e}}^*_{M_z}$, where $\hat{\mathbf{e}}_{M_z=0} = \hat{\mathbf{e}}_z$ and $\hat{\mathbf{e}}_{M_z=\pm1} = \mp(\hat{\mathbf{e}}_x \pm \mathrm{i}\hat{\mathbf{e}}_y)/\sqrt{2}$ are the unit vectors in the spherical representation. This accounts for the optical selection rules in the dipole approximation: the only optically active electron–hole pairs have $M_z = 0, \pm1$ and $M = 1$.

The absorption cross section of a nanocrystal at the transition frequency $\omega_{u,d}$ can be cast as

$$\sigma(\omega_{u,d}) = \frac{4\pi^2\omega_{u,d}}{\eta^2\hbar c}\left|\mathbf{e}_l\cdot\mathbf{D}_{u,d}\right|^2, \tag{16}$$

where $\mathbf{e}_l$ is the light polarization vector, η is the refractive index of the embedding matrix, and c is the speed of light in vacuum. The radiative lifetime of a vibron in the state u is given by

$$\tau_{\mathrm{u}} = \left(\sum_{\mathrm{d}}\frac{4\eta\omega^3_{u,d}\left|\mathbf{D}_{u,d}\right|^2}{3\hbar c^3}\right)^{-1}. \tag{17}$$

Within the excitonic picture, the direct optical transitions occur between the exciton vacuum G and the lowest excitons without a change of the vibrational state. Phonon-assisted transitions, in which the phonon population is different in the final state, is calculated by perturbation theory of the exciton–phonon interaction. In a vibron picture, all the transitions are treated on an equal footing, although for weak coupling the relative strength of the spectral lines should correspond to those of the excitonic picture plus perturbation theory. The excitonic picture breaks down when the gap between two exciton energy levels gets close to the optical phonon energy. In this case, non-adiabatic states appear and the vibron picture becomes indispensable. The contribution from every transition is weighted by the statistical factors affecting the initial states. In absorption, the probability of occurrence of the initial states with energy $E_{\mathrm{d}} = \sum_p n_{\mathrm{p}}\hbar\omega_{\mathrm{p}}$ is given by the Boltzmann distribution $P(E_{\mathrm{d}}) = Z^{-1}\exp(-E_{\mathrm{d}}/k_{\mathrm{B}}T)$, where the partition function, restricted to the *down* states, can be taken as $Z = \sum_{\mathrm{d}}\exp(-E_{\mathrm{d}}/k_{\mathrm{B}}T)$. At low temperature, the Boltzmann factors quench the transitions from initial excited phonon states. At room temperature, the optical phonon energy is comparable to $k_{\mathrm{B}}T$. Hence, one-phonon states, with slightly different energies, participate as initial states in the optical transitions. Moreover, these transitions make accessible the non-adiabatic vibron states with leading one-phonon partial DOSs which were discussed in section 3.2.

The calculated absorption spectrum at low temperature and room temperature of a model CdSe nanocrystal 2 nm in radius are shown in figure 4. The combined effects of dephasing by acoustic phonons and impurities, spectral jitter and jump, etc, are simulated, associating with each transition a lorentzian function with a uniform full width at half maximum that will be assumed to be 5 meV for 4 K and 50 meV for 300 K [24, 25]. At 4 K, the transitions occur from the ground state (without phonons) to the optically active vibron levels. Due to the fine structure of the exciton and vibron spectra, the peak positions depend on the angular

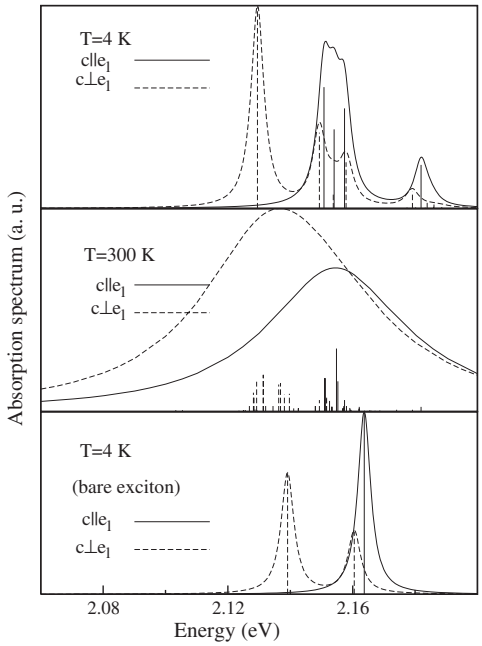

Figure 4. Fine structure of the absorption cross section of a single CdSe nanocrystal 2 nm in radius, calculated for the bare exciton at 4 K and for the vibrons at 4 and 300 K. The light electric field polarization vector $\mathbf{e}_l$ is parallel or perpendicular to the hexagonal c-axis of the nanocrystal. Vertical lines represent the different contributions to transitions.

momentum of the absorbed photon, i.e., its polarization. The lowest optically active level, at 2.129 eV, has $M_v = \pm 1$ and this transition is allowed for polarization perpendicular to the c-axis of the nanocrystal ($c \perp \mathbf{e}_l$). Photons with parallel polarization ($c \parallel \mathbf{e}_l$) are absorbed by $M_v = 0$ vibrons, the lowest one at 2.151 eV. Higher peaks correspond to transitions to higher vibron levels, including non-adiabatic ones. In the bottom of the figure is shown the spectrum calculated with the bare exciton model at 4 K. The 300 K spectrum of the bare exciton is the broadened convolution of the 4 K spectrum. The vibron model predicts several additional peaks due to non-adiabatic states, which in a simplified picture could be interpreted as replicas due to renormalized LO phonons [3]. At room temperature the transitions from phonon-populated *down* levels are activated. These transitions are included in the bare exciton model, but the spectrum does not change, because the electron and phonon systems are independent. In the full vibron model, the simple excitonic peaks are split in many close lines.

Figure 5 shows the emission spectrum calculated at 4 and 300 K with the full vibron model and at 300 K using the bare exciton model (i.e. dropping the exciton–phonon coupling). As will be argued below, at 4 K the emission can occur via phonon-assisted transitions and is outside the scope of a pure exciton model. In emission, the distribution function of a certain energy E_u is a complex and generally unknown function of the excitation power and the rates of relaxations, radiative and non-radiative recombinations. In the limit of fast relaxation compared with recombination and transitions to surface or external trap states, a quasi-equilibrium distribution function $P(E_\mathrm{u}) = Z_v^{-1} \exp(-E_\mathrm{u}/k_\mathrm{B}T)$, with $Z_v = \sum_u \exp(-E_\mathrm{u}/k_\mathrm{B}T)$, is reasonable. At low temperature, the thermal factors quench the transitions from higher vibron levels. The vertical full lines indicate the transitions responsible for the spectrum. In the framework of a pure exciton theory, the bright exciton $\pm 1^\mathrm{L}$ would be the emitting level. However,

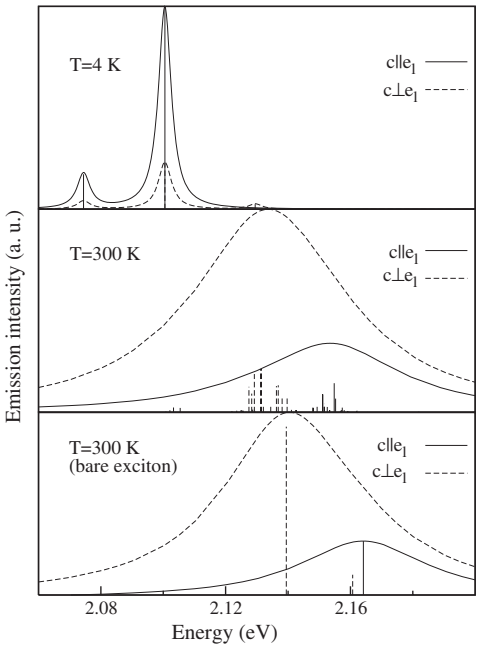

Figure 5. The same as in figure 4 for the emission spectrum.

it is considered that this state relaxes to the lower ± 2 dark exciton originating from the $(1s–1S_{3/2})_{2,\pm 2}$ EHP [12, 13, 26]. Hence, the luminescence of CdSe nanocrystals is attributed to a phonon-assisted recombination of this dark exciton and some other (still uncovered) mechanism for a weak zero-phonon line. In a vibronic model, this emission corresponds to a transition from the lowest $M_v = \pm 2$ vibron at 2.126 eV to one- and two-LO phonon *down* states, in a ratio of 83:17, emitting photons of 2.100 or 2.074 eV, respectively. This vibron has a recombination time of 1.3 μs, consistent in order of magnitude with the experimental data [12]. This state is responsible for the 4 K luminescence shown in figure 5. The one-phonon peak is due the phonons $(1, 2, \pm 1)$ for polarization perpendicular to the c-axis ($c \perp \mathbf{e}_l$) and the phonons $(1, 2, \pm 2)$ for parallel polarization ($c \parallel \mathbf{e}_l$). For both polarizations, the peak energies are coincident. At 4 K, the Boltzmann factors quench all the transitions from higher states. At 300 K, the transitions from the bright states, located at 3.5 meV above the dark level, become allowed and dominate the emission spectrum, increasing the emission intensity by a factor of 10^3 and shifting the peaks to the range of zero-phonon transitions. At this temperature, the peak energies for both polarizations differ because the emission is produced by different *up* states with $M_v = \pm 1$ and 0. These peaks have multiple contributions, including zero-phonon transitions and transitions from non-adiabatic *up* states to *down* levels with excited phonons. This can be compared with the simple picture of pure exciton transitions, shown in the bottom of figure 5.

In summary, we have implemented the direct calculation of the spectrum and the eigenstates of exciton–phonon complexes in CdSe nanocrystals, with possible applications to other compounds. We have found that the polaron correction to the exciton energy is significantly modified by the Coulomb interaction and a flexible wavefunction is needed even in the case of a nanocrystal radius smaller than the free exciton radius and infinite confinement potentials. We find that the virtual phonon number of the exciton polaron can be larger than 0.2, and also appear completely non-adiabatic states that have an important mixing of two-phonon states. This method opens a windows to investigate a rich spectrum of excitations that has been

largely dismissed. Further calculations for ensembles of nanocrystals are needed to verify if this improves the agreement of the theory with the experimental data.

Acknowledgments

This work has been supported by Fondecyt (Chile) under Grant No. 1050293. The Abdus Salam International Centre for Theoretical Physics is gratefully acknowledged for hosting one of the authors (EM-P) during part of this work and for computer resources. We also thank J Rössler, A Cabo, A González, and Al L Efros for useful comments.

Appendix A. Electronic states

Electronic excitations with an energy close to the gap are described by the exciton Hamiltonian, which can be cast as

$$H_{\mathrm{E}} = H_{\mathrm{e}} + H_{\mathrm{h}} + V_{\mathrm{eh}}, \tag{A.1}$$

where H_{e}, H_{h}, and V_{eh} are the electron and hole Hamiltonians, and the interaction operator, respectively. In the effective mass approximation, the electron Hamiltonian is given by

$$H_{\mathrm{e}} = \frac{\hat{\mathbf{p}}_{\mathrm{e}}^2}{2m_{\mathrm{e}}} + V_{\mathrm{e}}(r_{\mathrm{e}}), \tag{A.2}$$

m_{e} being the electron effective mass, and $V_{\mathrm{e}}(r_{\mathrm{e}})$ the confinement potential. The conduction band electron wavefunctions can be cast as

$$\langle \mathbf{r}|nlff_z\rangle = \sum_{l_z,s_z} \left(l\tfrac{1}{2}l_z s_z|ff_z\right) R_{nl}(r) Y_{ll_z}(\theta,\varphi)\,\langle \mathbf{r}|1/2,s_z\rangle\,, \tag{A.3}$$

where $(l\frac{1}{2}l_z s_z|ff_z)$ are the Clebsch–Gordan coefficients [27]. $\langle \mathbf{r}|1/2,s_z\rangle$ are the Γ_6 Bloch functions (with $\mathbf{s} = 1/2$ being the conduction band-edge angular momentum and $s_z = \pm 1/2$), s_z being the spin number. $R_{nl}(r)$ are the radial wavefunctions of a particle in the potential well $V_{\mathrm{e}}(r_{\mathrm{e}})$, and $Y_{ll_z}(\theta,\varphi)$ are the spherical harmonics [28]. The states have well-defined total ($\mathbf{f} = \mathbf{l} + \mathbf{s}$) angular momentum projection $\hbar f_z$ and square value $\hbar^2 f(f+1)$. Although the simpler l–s coupling can be used for the conduction band electrons, the l–f coupling scheme is a convenient way to build up the excitonic states in a spherical semiconductor nanocrystal. For the hole state, the l–f coupling scheme is imperative, so its use for both electrons and holes provides symmetry to the formula. Since the $s_z = \pm 1/2$ bands are uncoupled by the electron Hamiltonian (A.2), the states described by equation (A.3) have energies $E^e_{n,l}$ that are independent of the quantum numbers f, f_z. In the simulation of the real electronic states, the confinement potential is chosen as a spherical box with an effective radius R_{eff}, which is greater than the structural nanocrystal radius R. This effective radius is introduced in order to take into account, approximately, the penetration of the electron wavefunction in the surrounding medium. In our calculations, we determine R_{eff} from the condition that the energy of the 1s state $E_{1,0} = \hbar^2\pi^2/2m_{\mathrm{e}}R_{\mathrm{eff}}^2$ is equal to the energy calculated for a spherical well with a depth of $V_{\mathrm{e}} = 600$ meV [20]. Hence,

$$R_{nl}(r) = \sqrt{\frac{2}{R_{\mathrm{eff}}^3}}\frac{j_l(kr/R_{\mathrm{eff}})}{j_{l+1}(k)}, \qquad E_{nl} = \frac{\hbar^2 k^2}{2m_{\mathrm{e}}R_{\mathrm{eff}}^2}, \tag{A.4}$$

where k is the solution of $j_l(k) = 0$.

The hole states in the valence bands are described by a spherically symmetrized 4×4 $\mathbf{k} \cdot \mathbf{p}$ Hamiltonian [29–31]

$$H_{\mathrm{h}} = \frac{\gamma_1}{2m_0}\left[\hat{\mathbf{p}}_{\mathrm{h}}^2 - \frac{\mu}{9}\left(\mathbf{P}_{\mathrm{h}}^{(2)} \cdot \mathbf{J}^{(2)}\right)\right] + V_{\mathrm{h}}(r_{\mathrm{h}}) + V_{\mathrm{cf}}, \tag{A.5}$$

where $V_{\mathrm{h}}(r)$ is the confinement potential for the valence band, and $\mathbf{P}_{\mathrm{h}}^{(2)}$ and $\mathbf{J}^{(2)}$ are spherical tensors of rank 2 built from linear and angular momentum operators, $\mu = 2\gamma_2/\gamma_1$, and γ_2 and γ_1 are the Luttinger parameters of CdSe in the spherical approximation $\gamma_2 = \gamma_3$. V_{cf} is the crystal field operator for a wurtzite nanocrystal, which can be cast as [12]

$$V_{\mathrm{cf}} = -(\Delta/2)\left(J_z^2 - 1/4\right), \tag{A.6}$$

where Δ is the splitting of the top valence band in wurtzite bulk CdSe. This term only acts on the Bloch part of the hole wavefunction. V_{cf} breaks down the spherical symmetry and it would complicate unnecessarily the EHP basis functions. Instead of that, in this work V_{cf} is neglected to obtain the EHP basis states, and it is reintroduced at the later step of building the vibronic Hamiltonian.

The hole eigenfunctions in the L–F coupling scheme can be cast as

$$\langle \mathbf{r}|NLFF_z\rangle = \sum_{K=L,L+2}\sum_{L_z,J_z}\left(K\tfrac{3}{2}L_zJ_z|FF_z\right) \times R_{N,K}^{(F)}(r)Y_{KL_z}(\theta,\varphi)\,\langle \mathbf{r}|3/2,\,J_z\rangle\,, \tag{A.7}$$

where $\langle \mathbf{r}|3/2,\,J_z\rangle$ are the hole Bloch functions of the Γ_8 valence band with band-edge angular momentum $J = 3/2$. The hole Bloch functions result from the time-reversal operation on the valence electron Bloch functions, the phases of which are defined elsewhere [14]. For an abrupt confinement potential, the radial wavefunctions are similar to the electron functions for $F = 1/2$; for $F \geqslant 3/2$ they are given by

$$R_{N,L}^{(F)}(r) = A\left[j_{\mathrm{L}}(kr/R) - \frac{j_{\mathrm{L}}(\sqrt{\beta}kr/R)\,j_{\mathrm{L}}(k)}{j_{\mathrm{L}}(\sqrt{\beta}k)}\right], \tag{A.8a}$$

$$R_{N,L+2}^{(F)}(r) = -A\,(C_1+1)\,/C_2 \times \left[j_{L+2}(kr/R) - \frac{j_{L+2}(\sqrt{\beta}kr/R)\,j_{L+2}(k)}{j_{L+2}(\sqrt{\beta}k)}\right], \tag{A.8b}$$

where $\beta = m_{\mathrm{lh}}/m_{\mathrm{hh}}$, m_{hh} (m_{lh}) is the heavy (light) hole mass, and C_1 and C_2 are defined in [14]. The parameter k fulfills the transcendental equation,

$$j_{\mathrm{L}}(\sqrt{\beta}k)\,j_{L+2}(k)\,(C_1+1) = j_{L+2}(\sqrt{\beta}k)\,j_{\mathrm{L}}(k)\,(C_1-1)\,, \tag{A.9}$$

and A is a normalization constant, such that

$$\int\left[R_{N,L}^{(F)}(r)^2 + R_{N,L+2}^{(F)}(r)^2\right]r^2\,\mathrm{d}r = 1. \tag{A.10}$$

The hole energies are equal to $E_{\mathrm{h}} = \hbar^2k^2/2m_{\mathrm{hh}}R^2$.

The above states are denoted by the usual spectroscopy notation NA, with $A = S, P, D, \ldots$ ($s, p, d, \ldots$) for the $L = 0, 1, 2, \ldots$ ($l = 0, 1, 2\ldots$) hole (electron) states. In the case of the hole energies, the quantum number F is indicated by a sub-index, that is, NA_{F}.

The EHPs interact through the screened Coulomb and exchange interactions

$$V_{\mathrm{eh}} = V_{\mathrm{Coul}} + V_{\mathrm{exch}} = -\frac{e^2}{\epsilon_\infty|\mathbf{r}_{\mathrm{e}} - \mathbf{r}_{\mathrm{h}}|} - \frac{2}{3}\varepsilon_{\mathrm{exch}}a_0^3\delta(\mathbf{r}_{\mathrm{e}} - \mathbf{r}_{\mathrm{h}})\,(\boldsymbol{\sigma}\cdot\mathbf{J})\,, \tag{A.11}$$

where e, ϵ_∞, a_0 and $\varepsilon_{\mathrm{exch}}$ are the electron charge, the high-frequency dielectric constant, the lattice constant and the exchange strength parameter [12].

In the past, the exciton states have been obtained by using an expansion in a basis of EHP with the well-defined total angular momentum square $\hbar^2 M(M+1)$ and projection $\hbar M_z$

$$|\mu\rangle = |nNlLfF; MM_z\rangle = \sum_{f_z,F_z} (fFf_zF_z|MM_z)\,|nlff_z\rangle \otimes |NLFF_z\rangle\,. \tag{A.12}$$

In this work, we use the same states in the expansion for the vibron states. These EHP are briefly denoted by the combination of the electron and hole labels in spectroscopic notation, e.g. $1s–1S_{3/2}$. In the case that the angular momentum quantum numbers M and M_z need to be specified, they are indicated by sub-indices. The non-diagonal part of the exciton Hamiltonian is given by the matrix elements of the electron–hole interaction (A.11). An expression for the Coulomb part was reported in [17]. For the exchange interaction, the following expression is obtained by using the Wigner–Eckart theorem [27]:

$$\begin{aligned}\langle n'N'l'L'f'F'M'M'_z|V_{\rm exch}|nNlLfFMM_z\rangle = {} & -\frac{1}{\pi}\sqrt{\frac{5}{2}}\delta_{M,M'}\delta_{M_z,M'_z}\delta_{l,l'}(-1)^{F-F'+f-f'+l} \\ & \times (2f+1)(2f'+1)(2l+1)(2F+1)(2F'+1) \\ & \times \sum_{K,K'=L,L+2}\delta_{K,K'}\int R_{n'l'}(r)R_{nl}(r)R^{(F')}_{N'K'}(r)R^{(F)}_{NK}(r)r^2\,{\rm d}r \\ & \times W(ff'FF';1M)W(1/2\;1/2ff';1l) \\ & \times W(3/2\;3/2\;FF';1K)\sum_p(ll00|p0)(Kp00|K0)W(KKFF';p3/2) \\ & \times W(llff';p1/2)W(ff'FF';pM),\end{aligned} \tag{A.13}$$

where $W(abcd;ef)$ are the symbols of Racah [27].

For convenience, we include the effect of the valence crystal field splitting at this point. The matrix element can be cast as

$$\begin{aligned}\langle n'N'l'L'f'F'M'M'_z|V_{\rm cf}|nNlLfFMM_z\rangle = {} & -\frac{\Delta}{2}\delta_{n'N'l'L'f'F'M'M'_z;nNlLfFMM_z} \\ & -\Delta\delta_{M_z,M'_z}\delta_{n,l,f;n',l',f'}(-1)^{F+F'+f+1/2-M'_z}(MM'M_z-M_z|20) \\ & \times\sqrt{(2M+1)(2M'+1)(2F+1)(2F'+1)}\times W(FF'3/2\,3/2) \\ & \times\sum_{K,K'=L,L+2}(-1)^K\delta_{K,K'}W(MM'FF';2f)\int R^{(F')}_{N'K'}(r)R^{(F)}_{NK}(r)r^2\,{\rm d}r.\end{aligned} \tag{A.14}$$

The exciton matrix element $E_{\mu',\mu}$ (see equation (1)) are

$$E_{\mu',\mu} = (E_{\rm e}+E_{\rm h})\delta_{\mu',\mu} + \langle\mu'|V_{\rm Coul}+V_{\rm exch}+V_{\rm cf}|\mu\rangle. \tag{A.15}$$

Appendix B. Phonon states

The optical phonons are obtained from the continuum model of Trallero-Giner and Comas [32, 33]. For a spherical quantum dot, the optical phonons produce an oscillating electric potential with frequency [15]

$$\omega_{\rm p}^2 = \omega_{\rm L}^2 - \beta_{\rm L}^2\frac{\nu^2_{\tilde{n}_{\rm p},l_{\rm p}}}{R^2} \tag{B.1}$$

and spatial dependence

$$\phi_{\rm p}(\mathbf{r}) = \sqrt{\frac{\hbar}{2\omega_{\tilde{n}_{\rm p},l_{\rm p}}}}\frac{1}{\sqrt{R\rho}}\frac{4\pi\alpha}{\varepsilon_\infty}\Phi_{\tilde{n}_{\rm p},l_{\rm p}}(r)Y_{l_{\rm p},m_{\rm p}}(\vartheta,\varphi). \tag{B.2}$$

In the above formula, ω_{L}, β_{L}, ρ, and α are the longitudinal bulk phonon frequency at the Brillouin zone centre, the curvature parameter of the longitudinal bulk phonon dispersion law, the reduced mass density, and the electro-mechanics coupling parameter. The numbers $\nu_{\tilde{n}_{\mathrm{p}},l_{\mathrm{p}}}$ and the radial functions $\Phi_{\mathrm{p}}(r)$ are discussed elsewhere [15, 22].

The leading part of the exciton–phonon in polar semiconductors is effected via the electric potential ϕ, and the interaction matrix element is

$$\begin{aligned}\left\langle \mu' \left| H^{-}_{\mathrm{E-L}}(p) \right| \mu \right\rangle &= \left\langle \mu \left| H^{+}_{\mathrm{E-L}}(p) \right| \mu' \right\rangle^{*} \\ &= e \int \mathrm{d}^3\mathbf{r}_{\mathrm{e}}\, \mathrm{d}^3\mathbf{r}_{\mathrm{h}} \Psi^{*}_{\mu'}(\mathbf{r}_{\mathrm{e}}, \mathbf{r}_{\mathrm{h}}) \left[\phi_p(\mathbf{r}_{\mathrm{h}}) - \phi_{\mathrm{p}}(\mathbf{r}_{\mathrm{e}})\right] \Psi_{\mu}(\mathbf{r}_{\mathrm{e}}, \mathbf{r}_{\mathrm{h}}). \end{aligned} \tag{B.3}$$

An explicit expression for these matrix elements was reported in [17]. Details of our calculation of the optical phonons in CdSe nanocrystals can be found in [22].

References

[1] Trallero-Giner C, Cantarero A and Cardona M 1989 *Phys. Rev.* B **40** 4030
[2] Itoh T, Nishijima M, Ekimov A I, Gourdon C, Efros Al L and Rosen M 1995 *Phys. Rev. Lett.* **74** 1645
[3] Zimin L, Nair S V and Masumoto Y 1998 *Phys. Rev. Lett.* **80** 3105
[4] Fomin V M, Gladilin V N, Devreese J T, Pokatilov E P, Balaban S N and Klimin S N 1998 *Phys. Rev.* B **57** 2415
[5] Baranov A V, Yamaguchi S and Matsumoto Y 1997 *Phys. Rev.* B **56** 10332
[6] Inoue K, Toba K, Yamanaka A, Baranov A V, Onushchenko A A and Fedorov A V 1996 *Phys. Rev.* B **54** R8321
[7] Fedorov A V, Baranov A V and Inoue K 1997 *Phys. Rev.* B **56** 7491
[8] Oshiro K, Akai K and Matsuura M 1998 *Phys. Rev.* B **58** 7986
[9] Oshiro K, Akai K and Matsuura M 2002 *Phys. Rev.* B **66** 153308
[10] Vartanian A L, Asatryan A L and Kirakosyan A A 2002 *J. Phys.: Condens. Matter* **14** 13357
[11] Vasilevskiy M I, Anda E V and Makler S S 2004 *Phys. Rev.* B **70** 035318
[12] Efros Al L, Rosen M, Kuno M, Nirmal M, Norris D J and Bawendi M 1996 *Phys. Rev.* B **54** 4843
[13] Norris D J, Efros Al L, Rosen M and Bawendi M G 1996 *Phys. Rev.* B **53** 16347
[14] Menéndez-Proupin E and Trallero-Giner C 2004 *Phys. Rev.* B **69** 125336
[15] Roca E, Trallero-Giner C and Cardona M 1994 *Phys. Rev.* B **49** 13704
[16] Rodríguez-Suárez R, Menéndez-Proupin E, Trallero-Giner C and Cardona M 2000 *Phys. Rev.* B **62** 11006
[17] Menéndez-Proupin E and Cabo-Bisset N 2002 *Phys. Rev.* B **66** 085317
[18] Löwdin P-O 1951 *J. Chem. Phys.* **19** 1396
[19] Madelung O (ed) 1986 *Landolt-Börnstein Numerical Data and Functional Relationships in Science and Technology* vol III/22 (Berlin: Springer)
[20] Laheld U E H and Einevoll G T 1997 *Phys. Rev.* B **55** 5184
[21] Hermann C and Weisbuch C 1977 *Phys. Rev.* B **15** 823
[22] Menéndez-Proupin E, Trallero-Giner C and García-Cristobal A 1999 *Phys. Rev.* B **60** 5513
[23] Oshiro K, Akai K and Matsuura M 1999 *Phys. Rev.* B **59** 7986
[24] Müller J, Lupton J M, Rogach A L, Feldmann J, Talapin D V and Weller H 2004 *Phys. Rev. Lett.* **93** 167402
[25] Müller J, Lupton J M, Rogach A L, Feldmann J, Talapin D V and Weller H 2005 *Phys. Rev.* B **72** 205339
[26] Nirmal M, Norris D J, Kuno M, Bawendi M G, Efros Al L and Rosen M 1995 *Phys. Rev. Lett.* **75** 3728
[27] Brink D M and Satcher G R 1968 *Angular Momentum* (Oxford: Clarendon)
[28] Jackson J D 1962 *Classical Electrodynamics* (New York: Wiley)
[29] Baldereschi A and Lipari N O 1973 *Phys. Rev.* B **8** 2697
[30] Xia J-B 1989 *Phys. Rev.* B **40** 8500
[31] Efros Al L 1992 *Phys. Rev.* B **46** 7448
[32] Comas F and Trallero-Giner C 1993 *Physica* B **192** 394
[33] Trallero-Giner C and Comas F 1994 *Phil. Mag.* B **70** 583